Molecular Catalysis 475 (2019) 110461

Contents lists available at ScienceDirect

Molecular Catalysis

journal homepage: www.elsevier.com/locate/mcat

Zirconia phase effect in Pd/ZrO_2 catalyzed CO_2 hydrogenation into formate

Zhenhua Zhang[a,*], Liyuan Zhang[b], Max J. Hülsey[a], Ning Yan[a,*]

[a] Department of Chemical and Biomolecular Engineering, National University of Singapore, Blk E5, 4 Engineering Drive 4, 117585, Singapore
[b] Hefei National Laboratory for Physical Sciences at Microscale, CAS Key Laboratory of Materials for Energy Conversion and Department of Chemical Physics, University of Science and Technology of China, Hefei, 230026, PR China

ARTICLE INFO

Keywords:
CO_2
Support effect
Hydrogenation
Formic acid
Pd

ABSTRACT

In heterogeneous catalysis, transformation of CO_2 into formate largely relies on supported palladium catalyst, in which the support and in particular the support basicity plays a critical role. In this study, we prepared a series of Pd catalysts loaded on ZrO_2 bearing three different crystal phases, namely the tetragonal phase (ZrO_2-T), the monoclinic phase (ZrO_2-M), and the hybrid tetragonal and monoclinic phase (ZrO_2-M&T). With the same metal loading, ZrO_2-T supported Pd catalyst exhibited considerably higher intrinsic activity in CO_2 hydrogenation into formate compared with the other two catalysts. Pd/ZrO_2-T with 2 wt% Pd was the most active one in the series, affording a TOF of 2817 h^{-1} at 373 K. *In situ* DRIFTS spectroscopy, kinetic study and CO_2-TPD analysis provided evidence that all Pd/ZrO_2 catalysts follow a similar catalytic mechanism, and the origin of the superior activity for Pd/ZrO_2-T is the higher density of weak basic sites on ZrO_2-T, which facilitates the transformation of CO_2 into the desirable surface adsorbed bicarbonate as the precursor for formate. This work highlights the importance of crystal-phase engineering of the support in tuning the catalytic activity of Pd based catalysts for CO_2 hydrogenation.

1. Introduction

CO_2 is a useful C_1 feedstock to produce fuels and chemicals, such as alcohols, hydrocarbons and formic acid (HCOOH, FA) [1–19]. Among these, FA is an attractive non-toxic and non-flammable liquid product finding applications in leather tanning, silage preservation and also in hydrogen storage [20–22]. While the direct conversion of CO_2 and hydrogen to FA in the gas phase is thermodynamically unfavorable ($\Delta G = 33$ kJ mol^{-1}), the reaction readily occurs in aqueous phase with addition of base providing FA in the form of formate ($\Delta G = -4$ kJ mol^{-1}) [23]. Many efforts were devoted to produce formate using homogeneous catalysts, including Ir-, Ru-, Rh-, and Fe-based catalysts [23–32], which exhibited high reaction rates [33]. Heterogeneous catalysts have also aroused considerable interests, but their activity is often an order or orders of magnitude lower than the best homogeneous catalysts. Thus, the development of effective heterogeneous catalysts for CO_2 hydrogenation into formate is highly desirable.

Among various heterogeneous catalysts in the literature [8,9,34–52], Pd-based catalysts are most promising. The first reported heterogeneous catalyst was Pd black, dating back a century ago [38]. Afterwards, there was a long silent period in the area until more efficient Pd-based catalysts were developed recently. As an example, Pd/AC catalyst afforded a turnover frequency (TOF) of 527 h^{-1} using $NaHCO_3$ as carbon source and 2.75 MPa H_2 at 293 K [39]. Moreover, Lee et al. found the catalytic properties of Pd-based catalysts is significantly affected by the basicity of support, since basic sites help to stabilize reduced Pd species and to promote the formation of formate [42]. For the same reason, nitrogen doped carbon materials are widely used as support since the doped nitrogen sites are believed to facilitate CO_2 activation [48,49,53,54].

The crystal phase of the support may remarkably affect the performance of catalyst in hydrogenation reactions [55–58]. For instance, copper nanoparticles (NPs) supported on monoclinic phase ZrO_2 (ZrO_2-M) were found to be around 10 times more active compared to Cu supported on tetragonal phase ZrO_2 (ZrO_2-T) for the CO hydrogenation to methanol, which was assigned to the higher concentration of anionic vacancies and coordinatively unsaturated Lewis acid centres enhancing the adsorption of CO as HCOO-Zr groups [59,60]. The reverse effect was observed for copper supported on ZrO_2 for CO_2 hydrogenation to methanol where the improved activity of ZrO_2-T was assigned to stronger Cu-ZrO_2 interaction and a higher ratio of H/CO_2 on the surface [61,62]. Based on these previous investigations, ZrO_2, with tuneable basicity [63,64], was chosen as support to engineer an efficient Pd catalyst for formate formation.

Herein we report a systematic study to reveal how the crystal phases of ZrO_2 affect the activity of Pd/ZrO_2 catalyst in CO_2 hydrogenation to

* Corresponding authors.
E-mail addresses: hanyuzh@mail.ustc.edu.cn (Z. Zhang), ning.yan@nus.edu.sg (N. Yan).

https://doi.org/10.1016/j.mcat.2019.110461
Received 15 April 2019; Received in revised form 31 May 2019; Accepted 3 June 2019
Available online 19 June 2019

formate. The structure of Pd and the crystal phase of ZrO_2 both influence the catalytic performance of the catalyst. Metallic Pd promotes the H_2 dissociation, leading to enhanced hydrogenation ability at the Pd-ZrO_2 interface, while ZrO_2-T phase has a larger number of weak basic sites and thus provides more active sites to activate CO_2. Therefore, a 2%Pd/ZrO_2-T catalyst, which simultaneously contains metallic Pd and ZrO_2-T phase, exhibits a high activity with a TOF of ~2817 h^{-1} at 373 K.

2. Experimental

2.1. Catalyst preparation

Hybrid monoclinic and tetragonal phase was synthesized by a precipitation method. Typically, zirconium nitrate (2.0 mol/L) was dissolved into dilute nitric acid (5 wt%). Then ammonium hydroxide (4.0 M) was added slowly to the solution at room temperature under vigorous stirring till pH reached 10. The acquired solution was kept at room temperature for 5 h with a stirring rate of 400 rpm. Next, the resulting precipitate was filtered and washed with distilled water for 5 times until pH became 7. Finally, the solid was dried at 70 °C for 12 h and calcined at 500 °C for 6 h.

Various Pd/ZrO_2 catalysts were synthesized by a conventional precipitation-deposition method. In a typical procedure, ZrO_2 (200 mg) was dispersed in distilled water (100 mL) under ultrasound, in which ZrO_2-M and ZrO_2-T supports were purchased and ZrO_2-M&T support was synthesized experimentally. Then, an aqueous solution of Na_2CO_3 (1 mol/L) was added dropwise to a suspension mixture (100 mL) of $PdCl_2$ with different contents and ZrO_2 (200 mg) at 323 K until the pH value reached 10. The mixed solution was kept stirring for 3 h at 800 rpm. The resulting precipitate was acquired by centrifugation, and then washed with deionized water until no Cl^- can be detected. The solids were dried in an oven at 333 K for 12 h, calcined in air at 623 K for 2 h, and finally reduced in 5% H_2/N_2 flow (30 mL/min) at 473 K for 1 h.

2.2. Catalyst characterizations

The details for the inductively coupled plasma optical emission spectrometry (ICP-OES), powder X-ray diffraction (XRD), X-ray photoelectron spectroscopy (XPS), transmission electron microscopy (TEM), *in situ* diffuse reflectance infrared Fourier transformed spectroscopy (DRIFTS) and H_2-temperature programmed reduction (H_2-TPR) and CO_2-temperature programmed desorption (CO_2-TPD) studies are provided in the supporting information.

2.3. Catalytic evaluation

The CO_2 hydrogenation to FA was performed in the autoclave which is made by stainless steel and can bear the pressure up to 10 MPa. The autoclave can fill with 10 mL glass vial, in which contains the catalyst and reaction liquid. Before H_2 input, the autoclave is rinsed by 1 MPa H_2 for 20 times at room temperature. Before the catalytic tests, we first performed the reaction in different stirring rate ranging from 400 to 1200 rpm and proved that the mass transfer limitations can be neglected with 800 rpm stirring rate. Then we also changed the catalyst mass from 5 mg to 20 mg and found that the product formation rate (based on the total Pd atoms) and TOF (based on the surface Pd atoms) are both approximate, indicating that it is no mass transfer limitations in our reaction conditions. Consequently, 168 mg sodium bicarbonate is first dissolved into 2 mL H_2O to form a transparent solution using 10 mL glass vial. Then 20 mg catalysts are put into the glass vial and further untrasounded for 10 min to perfectly disperse the catalysts. For the test of catalytic performance, the reaction is conducted at 373 K for 1 h. When CO_2 was added into the feed gas, the autoclave was pressurized with the equal volumes of CO_2 and H_2 amounting to 4 MPa at room temperature (CO_2:H_2 = 1:1). The product (formate) was analyzed by High Performance Liquid Chromatography (HPLC, SHIMADZU, Singapore) equipped with a Hi-plex H column and RID detector. Repeating experiments suggest that the activity of a catalyst under a given condition is stable. Typically, the activity difference is within 5%. The recycling experiments were conducted according to the same procedure as described for the catalytic tests. The catalysts after reaction were washed by deionized water and dried in an oven at 333 K for the next batch use.

The apparent activation energy and the apparent kinetic orders of H_2 and bicarbonate on Pd/ZrO_2 on a given catalyst were measured using the same procedure as the test of catalytic performance. For apparent activation energy measurement, the reaction temperature was varied from 313 K to 343 K. The reaction order of H_2 was acquired by keeping the sodium bicarbonate mass as 168 mg but varying the H_2 pressure from 1 MPa to 2.5 MPa. The reaction order of sodium bicarbonate was acquired by keeping the H_2 pressure as 2 MPa but varying the sodium bicarbonate mass from 16.8 mg to 117.6 mg. All reactions were kept at a conversion less than 10%.

3. Results and discussion

Fig. 1 shows the XRD patterns of various ZrO_2 materials, which clearly reveal the crystal-phase structures of pure ZrO_2-M (JCPDS card NO. 37-1484), pure ZrO_2-T (JCPDS card NO. 65-2867), and a mixture of monoclinic and tetragonal phases (ZrO_2-M&T) [65]. The corresponding XPS spectra (Figure S1) show that the surfaces are exclusively composed of Zr(IV) features with the Zr $3d_{5/2}$ binding energy of 181.9 eV. Microscopic characterization results of various ZrO_2 further prove the successful acquisitions of ZrO_2-M with a lattice fringe of 3.7 Å (Fig. 2 A1 &A2), corresponding to monoclinic ZrO_2{110} crystal plane; ZrO_2-M&T with lattice fringes of 2.85 and 3.00 Å (Fig. 2 C1&C2), respectively corresponding to monoclinic ZrO_2{111} and tetragonal ZrO_2{101} crystal planes; and ZrO_2-T with a lattice fringe of 3.00 Å (Fig. 2 E1&E2), corresponding to tetragonal ZrO_2{101} crystal plane. Their corresponding specific BET surface areas were measured to be 103, 85, and 123 m^2/g, respectively. (Table S1)

The three ZrO_2 materials were applied to prepare ZrO_2-supported Pd catalysts (Pd/ZrO_2) by a conventional precipitation-deposition method. We denote the acquired Pd/ZrO_2 catalysts as x%Pd/ZrO_2-y, in which x represents the calculated weight percentage of Pd and y corresponds to the crystal-phase structure of ZrO_2. Table S1 summarizes the compositions of the Pd/ZrO_2 catalysts determined by ICP-OES. The actual Pd loadings on different catalysts are close to the predicted

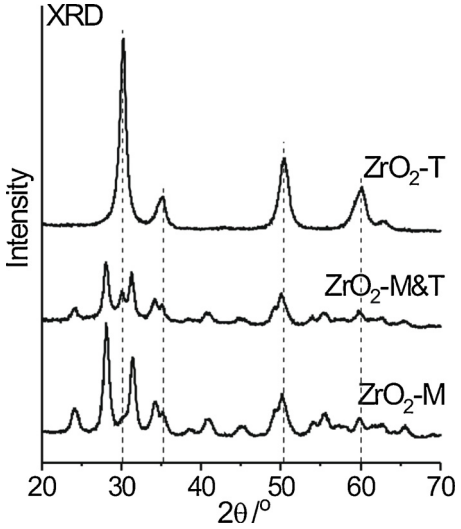

Fig. 1. XRD patterns of various ZrO_2 supports. The dash lines represent the diffraction peaks for tetragonal zirconia.

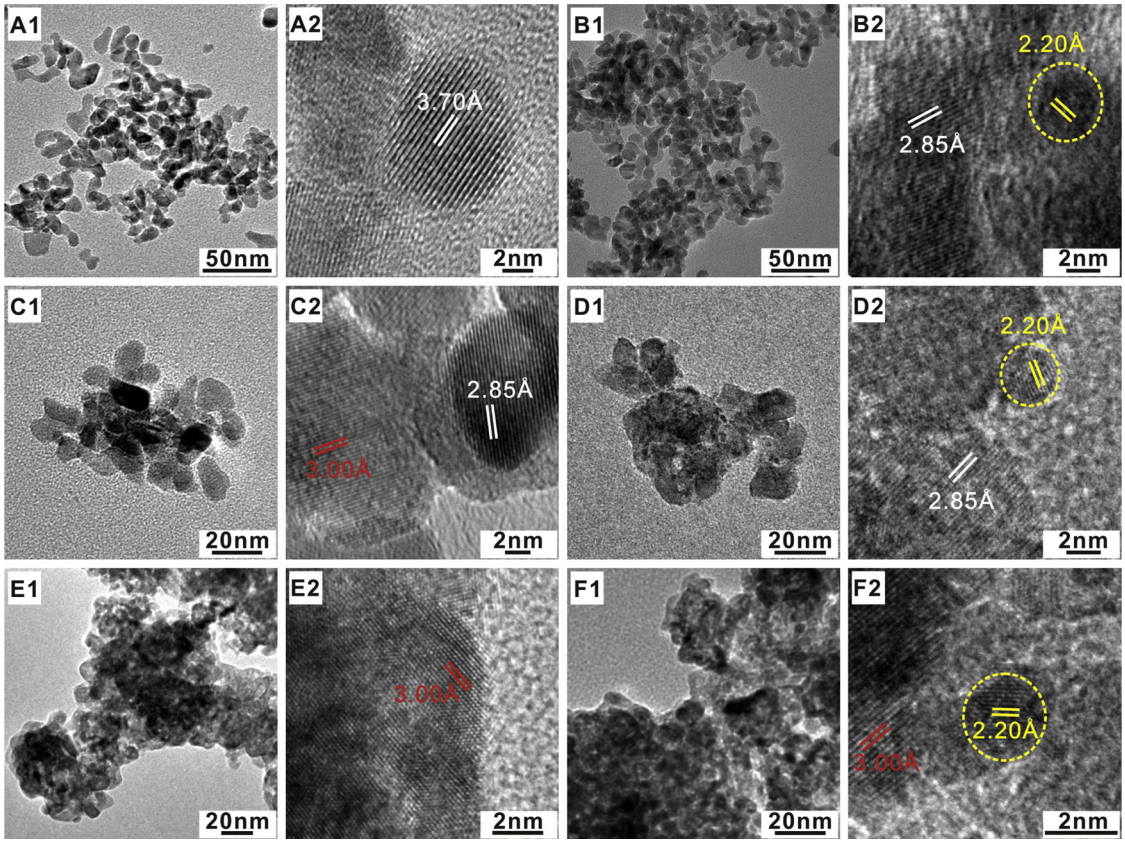

Fig. 2. TEM and HRTEM images of (A1, A2) ZrO_2-M, (B1, B2) 2%Pd/ZrO_2-M, (C1, C2) ZrO_2-M&T, (D1, D2) 2%Pd/ZrO_2-M&T, (E1, E2) ZrO_2-T, and (F1, F2) 2%Pd/ZrO_2-T catalysts. The lattice fringes of 2.85, 3.70, 3.00 and 2.20 Å correspond to the spacing of monoclinic ZrO_2{111} (JCPDS card NO. 37-1484), monoclinic ZrO_2{110}, tetragonal ZrO_2{101} (JCPDS card NO. 42-1164) and Pd{111} (JCPDS card NO. 65-2867) crystal planes respectively.

values based on the amount of Pd precursor, indicating that Pd was completely precipitated onto the supports.

The XRD patterns of all Pd/ZrO_2 catalysts (Figure S2) show the absence of Pd-associated diffraction patterns, suggesting the formation of either highly dispersed or amorphous Pd species. Meanwhile, the crystal-phase structures of various Pd/ZrO_2 catalysts are similar to their corresponding supports, except for the obvious weakening of ZrO_2-T phase on all Pd/ZrO_2-M&T catalysts, which may result from crystal transformation during the preparation process. As a result, the crystal-phase structures of acquired Pd/ZrO_2-M&T catalysts are similar to that of the Pd/ZrO_2-M catalysts. As shown in the TEM images (Fig. 2 and Figure S3-Figure S5), all acquired Pd/ZrO_2 catalysts well maintain their original ZrO_2 structures, in which Pd NPs were absent on catalysts with 0.01 wt% and 0.1 wt% Pd, but were easily recognized on 2%Pd/ZrO_2-M, 2%Pd/ZrO_2-M&T and 2%Pd/ZrO_2-T catalysts. The size distributions of Pd in the latter three samples are 3.4 ± 1.1, 3.0 ± 0.9 and 4.2 ± 0.7 nm, respectively (Figure S6). These results suggest the sizes of Pd can be adjusted by changing the Pd loading. The HRTEM images of various Pd/ZrO_2 catalysts reveal these NPs with a lattice fringe of 2.20 Å, which corresponds to the spacing of metallic Pd{111} crystal plane. The lattice fringes of ZrO_2-T phase are difficult to be identified on Pd/ZrO_2-M&T catalysts, consistent with the XRD results.

The surface compositions and structures of various Pd/ZrO_2 catalysts were further probed by XPS and *in situ* DRIFTS CO adsorption. Due to the strong interference from Zr 3p signal, Pd 3d XPS signals were only observed on 2 wt% Pd loading samples, in which two symmetric components with the Pd $3d_{5/2}$ binding energy of 335.9 and 337.6 eV appear and can be assigned respectively to metallic Pd and Pd(II) features (Fig. 3 A1-A3). This further demonstrates metallic Pd formed on 2 wt% Pd loading and the appearance of Pd(II) features may arise from Pd atoms of the interface between Pd NPs and ZrO_2, or from the oxidation of Pd NPs after catalysts exposure to air. The corresponding Zr 3d XPS spectra (Figure S7) show identical signals with the Zr $3d_{5/2}$ binding energy of 181.9 eV on all Pd/ZrO_2 catalysts.

In the *in situ* DRIFTS CO adsorption spectra (Fig. 3 B1-B3), CO adsorption peaks at 2080, 1920, and 1865 cm^{-1}, assignable to CO adsorbed onto linear, bridged, and 3-fold Pd^0 sites, respectively [66], were observed on Pd/ZrO_2 catalysts with 0.1 wt% and 2 wt% Pd loadings. The ratio of bridged/3-fold and linear Pd sites is higher on 2 wt% Pd loading, suggesting the size of Pd on 2 wt% Pd loading is larger than that on 0.1 wt% Pd loading samples [67]. When Pd loading is further decreased to 0.01 wt%, only linear CO adsorption peak is observed with peak position shift to 2090 cm^{-1}, indicating the formation of positively charged Pd species [68]. These prove that the size of Pd changes with the increase of Pd loading, from positively charged single-atom/cluster Pd species on 0.01%Pd/ZrO_2 to Pd NPs on 0.1%Pd/ZrO_2, and then to larger Pd NPs on 2%Pd/ZrO_2. Meanwhile, it is interesting to find that the CO adsorption peaks on various Pd/ZrO_2 catalysts are almost identical under the same Pd loading, indicating the structure of Pd is similar on ZrO_2 bearing varied phases.

Various Pd/ZrO_2 catalysts were evaluated in the catalytic reaction of CO_2 hydrogenation to formate. We first conducted CO_2 hydrogenation into formate under 2 MPa CO_2, 2 MPa H_2 at 373 K over the 2% Pd/ZrO_2 catalysts. $NaHCO_3$ was employed as a weak base. Interestingly, almost identical production rate of formate was observed when the CO_2 pressure decreased to zero (Figure S8), suggesting bicarbonate species to be the true precursor for formate formation (which was substantiated by *in situ* DRIFTS study using CO_2 as shown in later sections). Therefore, no gas-phase CO_2 is added for further activity comparison.

The catalytic performance of various Pd/ZrO_2 catalysts in $NaHCO_3$ hydrogenation to formate was evaluated. Pure ZrO_2 supports were inert, thus the catalytic performance is compared based on the amount

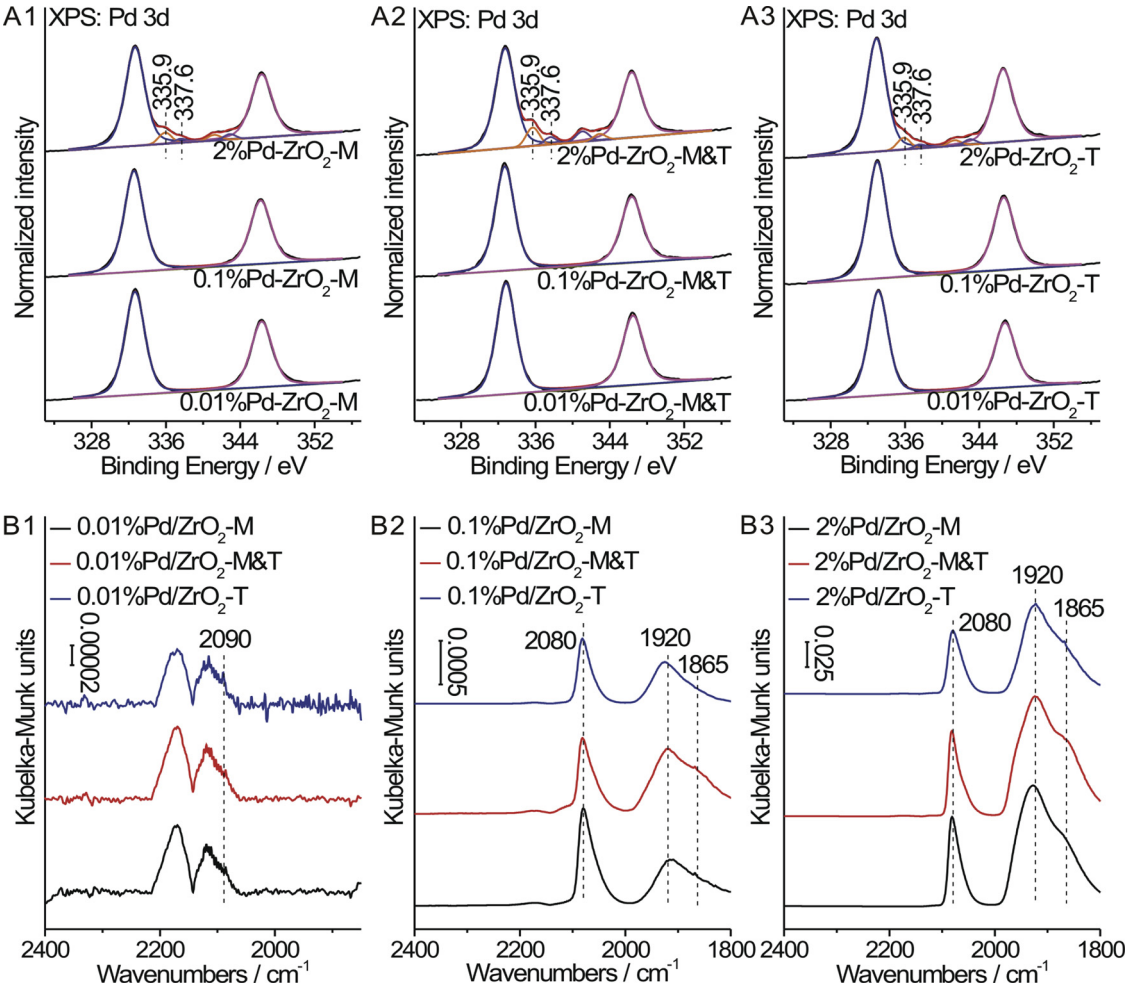

Fig. 3. (A1-A3) Pd 3d XPS spectra and (B1-B3) *in situ* DRIFTS of CO adsorption on various Pd/ZrO_2 catalysts at 298 K.

of Pd atoms. Fig. 4A shows the catalytic performance of various Pd/ZrO_2 catalysts normalized by the total amount of Pd atoms. The production rate of formate increases with the decrease of Pd loading on a particular ZrO_2 crystal phase, plausibly due to the increased dispersion of Pd at lower loadings. At the same Pd loading, the production rate of formate follows the order of Pd/ZrO_2-T > Pd/ZrO_2-M&T > Pd/ZrO_2-M. Pd supported on ZrO_2-T is always two times more active than Pd on ZrO_2-M&T, while Pd/ZrO_2-M&T is about 50% more active than Pd/ZrO_2-M. The TOF values of 2 wt% Pd catalysts were further obtained from estimation of surface Pd atoms based on the average particle size in TEM analysis (Figure S6). Indeed, $2\%Pd/ZrO_2$-T catalyst shows more than 2 times higher TOF numbers (2817 h^{-1}) than the $2\%Pd/ZrO_2$-M (1301 h^{-1}) and $2\%Pd/ZrO_2$-M&T catalysts (1291 h^{-1}) (Fig. 4D). Of note, 93% of the original reaction activity was preserved after 5 cycles for both $2\%Pd/ZrO_2$-M and $2\%Pd/ZrO_2$-T catalysts (Figure S12), suggesting the high stability of the Pd/ZrO_2 catalysts.

The apparent activation energy (E_a) calculated based on the Arrhenius plots (Fig. 4B&C and Figure S9) show a monotonic decrease of E_a when Pd loading increases from 0.01 wt% to 0.1 wt% and then to 2 wt%. On one hand, it indicates that 2 wt% Pd loadings are intrinsically more active on different ZrO_2, suggesting that metallic Pd is favourable for the formate formation. On the other hand, at the same Pd loading E_a is very close to each other for Pd catalysts supported on different ZrO_2 suggesting the phase of zirconia does not considerably affect the electronic structure of Pd. For instance, E_a values for both $0.01\%Pd/ZrO_2$-T and $0.01\%Pd/ZrO_2$-T are at around 40 kJ/mol, while the values for both $2\%Pd/ZrO_2$-T and $2\%Pd/ZrO_2$-T are slightly higher than 20 kJ/mol. As such, we conclude the significantly different TOF values are induced by the different number of active sites in different ZrO_2 support.

The $2\%Pd/ZrO_2$-M and $2\%Pd/ZrO_2$-T catalysts are chosen for further kinetic investigations. The reaction order of H_2 (Fig. 4E and Figure S10) is similar on both catalysts, exhibiting a slightly positive order of around 0.2, suggesting H_2 activation is unlikely to be the rate-limiting step. In contrast, the reaction order of bicarbonate (since its concentration is easier to control compared with CO_2) on $2\%Pd/ZrO_2$-M catalyst (1.19 ± 0.08) is higher than that on $2\%Pd/ZrO_2$-T catalyst (0.73 ± 0.02) (Fig. 4F and Figure S11), indicating their different catalytic performance is associated with the activation of CO_2. It has been reported that CO_2 prefers to bind with metal oxide to start a catalytic cycle. Plausibly, ZrO_2-T phase binds CO_2 more favourably than ZrO_2-M for the hydrogenation reaction to formate.

Subsequently, CO_2-TPD measurements were performed to probe the basicity of different supports. Various pure ZrO_2 support exhibit similar desorption temperature of CO_2 starting at 315 K (Fig. 5A and Table S1), indicating that they all bear similarly weak basic sites. On the contrary, the amount of basic sites is different, following the order of ZrO_2-T > ZrO_2-M&T > ZrO_2-M, similar to the reported results [69]. The CO_2-TPD results of various $2\%Pd/ZrO_2$ catalysts are slightly different. First, the amount of weak basic sites on $2\%Pd/ZrO_2$-M&T catalyst is lower than that on $2\%Pd/ZrO_2$-M catalyst, which can be explained by the larger particle size of ZrO_2-M&T catalyst (Fig. 2). Second, a new desorption peak of CO_2, starting at 480 K (reflecting strong basicity), only appears on $2\%Pd/ZrO_2$-M&T and $2\%Pd/ZrO_2$-M catalysts, not on the best performed $2\%Pd/ZrO_2$-T catalyst. Thus, it is inferred from the CO_2-TPD results that the catalytic performance of CO_2 hydrogenation to

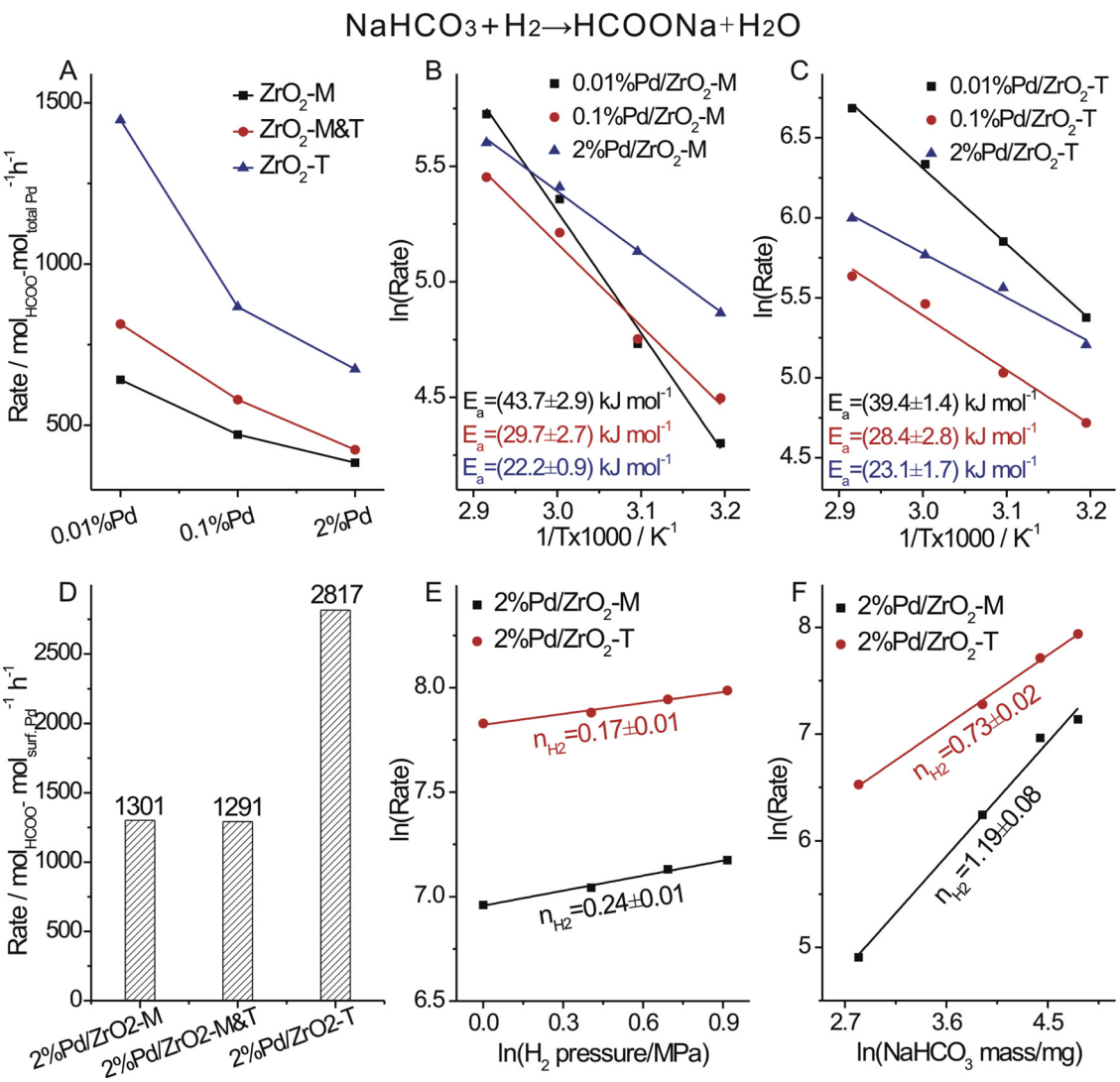

Fig. 4. Chemical equation of formate formation shown on the title. (A) Production rate (mol_{HCOO-} $mol_{total\ Pd}{}^{-1}$ h^{-1}) of formate on various Pd/ZrO_2 catalysts based on the total amount of Pd atoms; Arrhenius plots of various (B) Pd/ZrO_2-M and (C) Pd/ZrO_2-T catalysts; (D) Production rate (mol_{HCOO-} $mol_{surf.\ Pd}{}^{-1}$ h^{-1}) of formate on representative various 2%Pd/ZrO_2 catalysts based on the surface Pd atoms; Reaction orders of (E) bicarbonate and (F) H_2 of 2%Pd/ZrO_2-M and 2%Pd/ZrO_2-T catalysts.

formate on various Pd/ZrO_2 catalysts is strongly dependent on the density and strength of the basicity of the support. While higher density of basic sites is desirable for CO_2 adsorption, only CO_2 bound on weak basic sites can be easily further transformed into formate.

In the H_2-TPR results (Fig. 5 B–D), no reduction peak was observed for pure ZrO_2. For various calcined Pd/ZrO_2 catalysts, no reduction signal was observed for Pd at 0.01 wt% loading. A broad reduction peak starting from 525 K appears on 0.1 wt% Pd loadings, which is assigned to the reduction of PdO-ZrO_2 interface [70]. The reduction temperature of PdO-ZrO_2 interface shifts to 480 K when the Pd loading further increases to 2 wt%, accompanied by a new reduction peak at an even lower temperature, which can be ascribed to the reduction of PdO [70]. The H_2-TPR result clearly reveals the reaction properties with H_2 on various Pd/ZrO_2 catalysts are dependant with the loading of Pd, not with the crystal phase of the ZrO_2 support.

The reaction mechanism of CO_2 hydrogenation to formate catalysed by 2%Pd/ZrO_2-M and 2%Pd/ZrO_2-T catalysts was studied by *in situ* DRIFTS. Fig. 6 shows the *in situ* time-resolved DRIFTS results of the two catalysts under one bar CO_2 and H_2 mixture (CO_2:H_2 = 1:1) at 373 K. The band assignments are summarized in Table S2. Similar surface species, including monodentate carbonate (1354–1358 and 1439-1459 cm^{-1}), bidentate carbonate (1304–1316, 1510–1541, and 1684-1691 cm^{-1}), bicarbonate (1470–1487 and 1613-1630 cm^{-1}), and formate (1375–1380 and 1595-1599 cm^{-1}) [71–76], are generated on two catalysts with different ratios. The ratio of formate on 2%Pd/ZrO_2-T catalyst is much higher than that on 2%Pd/ZrO_2-M catalyst, which is consistent with their catalytic performance. Other vibrational bands at 1841–1848, 1900–1908, and 2018-2037 cm^{-1} can be assigned to CO adsorption on Pd NPs [66]. The formation of CO may arise from the by-product of CO_2 hydrogenation to FA or the decomposition of formed FA. Meanwhile, their positions shift towards higher wavenumbers as the reaction proceeds, indicating the wavenumbers increase with the CO coverage. It also explains why the wavenumbers of CO vibrational bands under reaction condition are lower than those obtained in the *in situ* DRIFTS CO adsorption experiments conducted under a higher CO coverage (Fig. 3 B1-B3). *In situ* time-resolved DRIFTS spectra of the stepwise treatment of the catalysts by CO_2 or H_2 are shown in Figure S13. The surface species were firstly generated under pure CO_2 or H_2 stream for 30 min at 373 K and then the other gas was introduced. The results reveal bidentate carbonate and bicarbonate are the main surface species on both fresh catalysts under pure CO_2 atmosphere. Upon H_2 introduction, the amount of bicarbonate and surface-bound formate

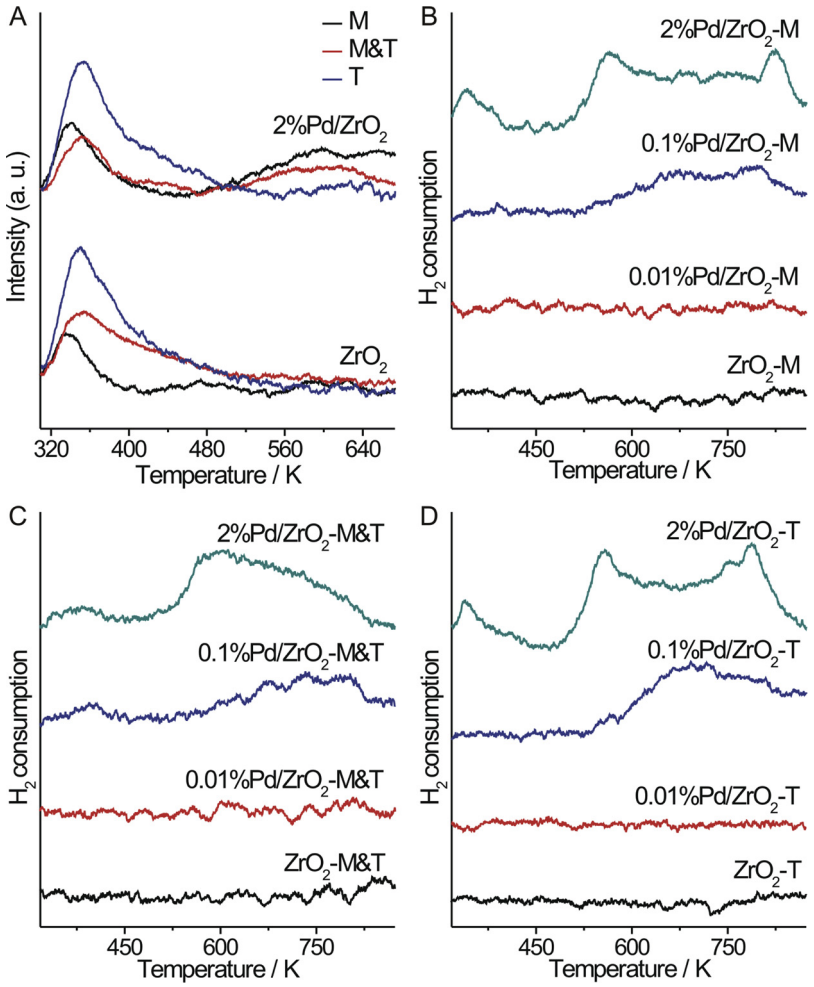

Fig. 5. (A) CO_2-TPD profiles of various ZrO_2 and Pd/ZrO_2 catalysts; H_2-TPR profiles of (B) ZrO_2-M and various Pd/ZrO_2-M catalysts, (C) ZrO_2-M&T and various Pd/ZrO_2-M&T catalysts, and (D) ZrO_2-T and various Pd/ZrO_2-T catalysts.

increase at the expense of surface bidentate carbonate on 2%Pd/ZrO_2-M catalyst (Figure S13 A1), while formate formation accompanied by the decrease of both bidentate carbonate and bicarbonate species was observed on 2%Pd/ZrO_2-T catalyst (Figure S13 B1). When H_2 is introduced first, weak desorption of bicarbonate on 2%Pd/ZrO_2 catalyst and bicarbonate/formate on 2%Pd/ZrO_2-T catalyst is generated, accompanied by the consumption of surface monodentate carbonate and bidentate carbonate species originally presented in the catalysts (Figure S13 A2&B2). Based on these, it appears that the catalytic mechanism for both catalysts is similar, that is, CO_2 reacts with the support to form adsorbed bidentate carbonate, and subsequently to bicarbonate species and formate species by stepwise H transfer. Another useful information from *in situ* DRIFT study is that CO is only generated under H_2 atmosphere, indicating that its formation perhaps is due to the hydrodeoxygenation of surface carbonate, not from FA decomposition.

In summary, a series of ZrO_2-M, ZrO_2-M&T, and ZrO_2-T supported Pd catalysts were synthesized, which exhibited a distinct crystal-phase-dependent catalytic performance in the hydrogenation of CO_2 to formate. Under the same Pd loading, Pd supported on ZrO_2-T phase is much more active than Pd supported on ZrO_2-M and ZrO_2-M&T phases. The best 2%Pd/ZrO_2-T catalyst afforded a high activity with TOFs close to 3000 h^{-1} in the presence of 2 MPa CO_2, 2 MPa H_2 at 373 K, higher

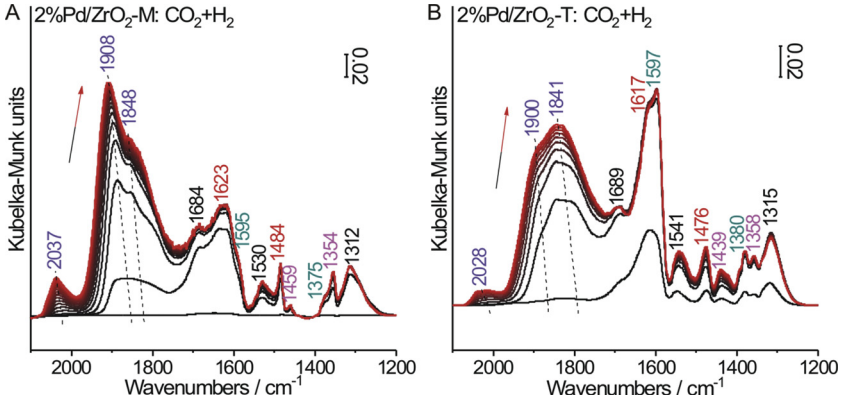

Fig. 6. *In situ* time-resolved DRIFTS spectra of CO_2 hydrogenation reaction (CO_2:H_2 = 1:1) on (A) 2%Pd/ZrO_2-M and (B) 2%Pd/ZrO_2-T catalysts at 373 K. Duration of the measurement is one hour and the colored arrow indicates the time progress. Time interval between two adjacent spectra is around three minutes. Wavenumbers indicated at the plots are color-coded as follows: Purple – CO, Black – bidentate carbonate, Red – bicarbonate, turquoise – formate and pink – monodentate carbonate. (For interpretation of the references to colour in this figure legend, the reader is referred to the web version of this article).

than a majority of existing reports under similar reaction conditions. The catalyst is also stable, maintaining 93% of initial activity after 5 cycles. *In situ* DRIFTS results reveal that the reaction follows the same mechanism on both Pd/ZrO_2-M and Pd/ZrO_2-T catalysts, in which stepwise hydrogenation of surface adsorbed CO_2 leads to formate formation. Kinetic study, combined with CO_2-TPD and H_2-TPR techniques, suggested CO_2 activation to be the rate-determining step, and that the different activity of $2\%Pd/ZrO_2$ catalyst is associated with the differences in the density of weak basic sites on the support. This study adds insights into the catalytic mechanism of Pd-based catalysts in CO_2 hydrogenation, and highlights the importance of crystal phase engineering of the support to improve the catalyst for FA synthesis.

Acknowledgement

We thank the NUS Flagship Green Energy Programme for the financial support.

Appendix A. Supplementary data

Supplementary material related to this article can be found, in the online version, at doi:https://doi.org/10.1016/j.mcat.2019.110461.

References

[1] M. Mikkelsen, M. Jørgensen, F.C. Krebs, The teraton challenge. A review of fixation and transformation of carbon dioxide, Energy Environ. Sci. 3 (2010) 43–81.
[2] H. Yang, Z. Xu, M. Fan, R. Gupta, R.B. Slimane, A.E. Bland, I. Wright, Progress in carbon dioxide separation and capture: a review, J. Environ. Sci. 20 (2008) 14–27.
[3] E.J. Choi, Y.H. Lee, D.-W. Lee, D.-J. Moon, K.-Y. Lee, Hydrogenation of CO2 to methanol over Pd–Cu/CeO2 catalysts, Mol. Catal. 434 (2017) 146–153.
[4] M. Sadeghinia, A. Nemati Kharat Ghaziani, M. Rezaei, Component ratio dependent Cu/Zn/Al structure sensitive catalyst in CO2/CO hydrogenation to methanol, Mol. Catal. 456 (2018) 38–48.
[5] F.C.F. Marcos, J.M. Assaf, E.M. Assaf, CuFe and CuCo supported on pillared clay as catalysts for CO2 hydrogenation into value-added products in one-step, Mol. Catal. 458 (2018) 297–306.
[6] N. Yan, K. Philippot, Transformation of CO2 by using nanoscale metal catalysts: cases studies on the formation of formic acid and dimethylether, Curr. Opin. Chem. Eng. 20 (2018) 86–92.
[7] W. Wang, S. Wang, X. Ma, J. Gong, Recent advances in catalytic hydrogenation of carbon dioxide, Chem. Soc. Rev. 40 (2011) 3703–3727.
[8] A. Álvarez, A. Bansode, A. Urakawa, A.V. Bavykina, T.A. Wezendonk, M. Makkee, J. Gascon, F. Kapteijn, Challenges in the greener production of formates/formic acid, methanol, and DME by heterogeneously catalyzed CO2 hydrogenation processes, Chem. Rev. 117 (2017) 9804–9838.
[9] G.H. Gunasekar, K. Park, K.-D. Jung, S. Yoon, Recent developments in the catalytic hydrogenation of CO2 to formic acid/formate using heterogeneous catalysts, Inorg. Chem. Front. 3 (2016) 882–895.
[10] M. Hulla, G. Laurenczy, P.J. Dyson, Mechanistic study of the N-Formylation of amines with carbon dioxide and hydrosilanes, ACS Catal. 8 (2018) 10619–10630.
[11] Y. Gu, K. Matsuda, A. Nakayama, M. Tamura, Y. Nakagawa, K. Tomishige, Direct synthesis of alternating polycarbonates from CO2 and diols by using a catalyst system of CeO2 and 2-Furonitrile, ACS Sustain. Chem. Eng. 7 (2019) 6304–6315.
[12] M. Tamura, A. Miura, M. Honda, Y. Gu, Y. Nakagawa, K. Tomishige, Direct catalytic synthesis of N-Arylcarbamates from CO2, anilines and alcohols, ChemCatChem 10 (2018) 4821–4825.
[13] M. Tamura, K. Ito, Y. Nakagawa, K. Tomishige, CeO2-catalyzed direct synthesis of dialkylureas from CO2 and amines, J. Catal. 343 (2016) 75–85.
[14] I. Kim, G. Lee, H. Jeong, J.H. Park, J.C. Jung, Bifunctionality of Cu/ZnO catalysts for alcohol-assisted low-temperature methanol synthesis from syngas: effect of copper content, J. Energy Chem. 26 (2017) 373–379.
[15] Y. Jeong, I. Kim, J.Y. Kang, N. Yan, H. Jeong, J.K. Park, J.H. Park, J.C. Jung, Effect of the aging time of the precipitate on the activity of Cu/ZnO catalysts for alcohol-assisted low temperature methanol synthesis, J. Mol. Catal. A Chem. 418-419 (2016) 168–174.
[16] M.M. Taqui Khan, S.B. Halligudi, S. Shukla, Stoichiometric reduction of carbon dioxide to HCHO and HCOOH by K [Ru^{III}(EDTA-H)Cl]·$2H_2O$.", J. Mol. Catal. 53 (1989) 305–313.
[17] M.M. TaquiKhan, S.B. Halligudi, N. Nageswara Rao, S. Shukla, Formic acid and formaldehyde as spin-off products in RU-EDTA-CO complex catalyzed liquid phase water-gas shift (WGS) reaction, J. Mol. Catal. 51 (1989) 161–170.
[18] N. Roy, N. Suzuki, C. Terashima, A. Fujishima, Recent Improvements in the production of solar fuels: from CO_2 reduction to water splitting and artificial photosynthesis, Bull. Chem. Soc. Jpn. 92 (2019) 178–192.
[19] K. Maeda, T.E. Mallouk, Two-dimensional metal oxide nanosheets as building blocks for artificial photosynthetic assemblies, Bull. Chem. Soc. Jpn. 92 (2019) 38–54.
[20] W. Reutemann, H. Kieczka, Formic Acid. Ullmann's Encyclopedia of Industrial Chemistry, (2000).
[21] A. Boddien, C. Federsel, P. Sponholz, D. Mellmann, R. Jackstell, H. Junge, G. Laurenczy, M. Beller, Towards the development of a hydrogen battery, Energy Environ. Sci. 5 (2012) 8907–8911.
[22] S. Enthaler, J. von Langermann, T. Schmidt, Carbon dioxide and formic acid—the couple for environmental-friendly hydrogen storage? Energy Environ. Sci. 3 (2010) 1207–1217.
[23] S. Moret, P.J. Dyson, G. Laurenczy, Direct synthesis of formic acid from carbon dioxide by hydrogenation in acidic media, Nat. Commun. 5 (2014) 4017.
[24] W.-H. Wang, J.F. Hull, J.T. Muckerman, E. Fujita, Y. Himeda, Second-coordination-sphere and electronic effects enhance iridium(iii)-catalyzed homogeneous hydrogenation of carbon dioxide in water near ambient temperature and pressure, Energy Environ. Sci. 5 (2012) 7923–7926.
[25] A. Urakawa, F. Jutz, G. Laurenczy, A. Baiker, Carbon dioxide hydrogenation catalyzed by a ruthenium dihydride: a DFT and high-pressure spectroscopic investigation, Chem. Eur. J. 13 (2007) 3886–3899.
[26] Y. Musashi, S. Sakaki, Theoretical study of rhodium(III)-catalyzed hydrogenation of carbon dioxide into formic acid. Significant differences in reactivity among rhodium(iii), rhodium(i), and ruthenium(ii) complexes, J. Am. Chem. Soc. 124 (2002) 7588–7603.
[27] Y. Zhang, A.D. MacIntosh, J.L. Wong, E.A. Bielinski, P.G. Williard, B.Q. Mercado, N. Hazari, W.H. Bernskoetter, Iron catalyzed CO2 hydrogenation to formate enhanced by Lewis acid co-catalysts, Chem. Sci. 6 (2015) 4291–4299.
[28] C.A. Huff, M.S. Sanford, Catalytic CO2 hydrogenation to formate by a ruthenium pincer complex, ACS Catal. 3 (2013) 2412–2416.
[29] C. Federsel, R. Jackstell, A. Boddien, G. Laurenczy, M. Beller, Ruthenium-catalyzed hydrogenation of bicarbonate in water, ChemSusChem 3 (2010) 1048–1050.
[30] S. Thomas, R.A. Paciello, A process for the synthesis of formic acid by CO2 hydrogenation: thermodynamic aspects and the role of CO, Angew. Chem. Int. Ed. 50 (2011) 7278–7282.
[31] F. Hutschka, A. Dedieu, M. Eichberger, R. Fornika, W. Leitner, Mechanistic aspects of the rhodium-catalyzed hydrogenation of CO2 to formic acid-a theoretical and kinetic study, J. Am. Chem. Soc. 119 (1997) 4432–4443.
[32] Z. Xu, N.D. McNamara, G.T. Neumann, W.F. Schneider, J.C. Hicks, Catalytic hydrogenation of CO2 to formic acid with silica-tethered iridium catalysts, ChemCatChem 5 (2013) 1769–1771.
[33] A. Behr, P. Neubert, Applied Homogeneous Catalysis, John Wiley & Sons, 2012.
[34] D. Preti, C. Resta, S. Squarcialupi, G. Fachinetti, Carbon dioxide hydrogenation to formic acid by using a heterogeneous gold catalyst, Angew. Chem. Int. Ed. 50 (2011) 12551–12554.
[35] G.A. Filonenko, W.L. Vrijburg, E.J.M. Hensen, E.A. Pidko, On the activity of supported Au catalysts in the liquid phase hydrogenation of CO2 to formates, J. Catal. 343 (2016) 97–105.
[36] C. Hao, S. Wang, M. Li, L. Kang, X. Ma, Hydrogenation of CO2 to formic acid on supported ruthenium catalysts, Catal. Today 160 (2011) 184–190.
[37] K. Mori, T. Taga, H. Yamashita, Isolated single-atomic Ru catalyst bound on a layered double hydroxide for hydrogenation of CO2 to formic acid, ACS Catal. 7 (2017) 3147–3151.
[38] G. Bredig, S.R. Carter, Katalytische synthese der ameisensäure unter druck, Ber. Dtsch. Chem. Ges. 47 (1914) 541–545.
[39] J. Su, L. Yang, M. Lu, H. Lin, Highly efficient hydrogen storage system based on ammonium bicarbonate/formate redox equilibrium over palladium nanocatalysts, ChemSusChem 8 (2015) 813–816.
[40] J. Su, M. Lu, H. Lin, High yield production of formate by hydrogenating CO2 derived ammonium carbamate/carbonate at room temperature, Green Chem. 17 (2015) 2769–2773.
[41] Q.-Y. Bi, J.-D. Lin, Y.-M. Liu, X.-L. Du, J.-Q. Wang, H.-Y. He, Y. Cao, An aqueous rechargeable formate-based hydrogen battery driven by heterogeneous Pd catalysis, Angew. Chem. Int. Ed. 53 (2014) 13583–13587.
[42] J.H. Lee, J. Ryu, J.Y. Kim, S.-W. Nam, J.H. Han, T.-H. Lim, S. Gautam, K.H. Chae, C.W. Yoon, Carbon dioxide mediated, reversible chemical hydrogen storage using a Pd nanocatalyst supported on mesoporous graphitic carbon nitride, J. Mater. Chem. A 2 (2014) 9490–9495.
[43] K. Mori, T. Sano, H. Kobayashi, H. Yamashita, Surface engineering of a supported PdAg catalyst for hydrogenation of CO2 to formic acid: elucidating the active Pd atoms in alloy nanoparticles, J. Am. Chem. Soc. 140 (2018) 8902–8909.
[44] M.S. Maru, S. Ram, R.S. Shukla, N.-u.H. Khan, Ruthenium-hydrotalcite (Ru-HT) as an effective heterogeneous catalyst for the selective hydrogenation of CO2 to formic acid, Mol. Catal. 446 (2018) 23–30.
[45] X. Lv, G. Lu, Z.-Q. Wang, Z.-N. Xu, G.-C. Guo, Computational evidence for Lewis base-promoted CO2 hydrogenation to formic acid on gold surfaces, ACS Catal. 7 (2017) 4519–4526.
[46] X. Yang, S. Kattel, S.D. Senanayake, J.A. Boscoboinik, X. Nie, J. Graciani, J.A. Rodriguez, P. Liu, D.J. Stacchiola, J.G. Chen, Low pressure CO2 hydrogenation to methanol over gold nanoparticles activated on a CeOx/TiO2 interface, J. Am. Chem. Soc. 137 (2015) 10104–10107.
[47] Q. Liu, X. Yang, L. Li, S. Miao, Y. Li, Y. Li, X. Wang, Y. Huang, T. Zhang, Direct catalytic hydrogenation of CO2 to formate over a Schiff-base-mediated gold nanocatalyst, Nat. Commun. 8 (2017) 1407.
[48] S. Masuda, K. Mori, Y. Futamura, H. Yamashita, PdAg nanoparticles supported on functionalized mesoporous carbon: promotional effect of surface amine groups in reversible hydrogen delivery/storage mediated by formic acid/CO2, ACS Catal. 8 (2018) 2277–2285.
[49] W. Fanan, X. Jinming, S. Xianzhao, S. Xiong, H. Yanqiang, Z. Tao, Palladium on nitrogen-doped mesoporous carbon: a bifunctional catalyst for formate-based,

carbon-neutral hydrogen storage, ChemSusChem 9 (2016) 246–251.
[50] X. Shao, X. Yang, J. Xu, S. Liu, S. Miao, X. Liu, X. Su, H. Duan, Y. Huang, T. Zhang, Iridium single-atom catalyst performing a quasi-homogeneous hydrogenation transformation of CO < sub > 2 < /sub > to formate, Chem 5 (2019) 693–705.
[51] W.-T. Lee, A.P. van Muyden, F.D. Bobbink, Z. Huang, P.J. Dyson, Indirect CO2 methanation: hydrogenolysis of cyclic carbonates catalyzed by Ru-Modified zeolite produces methane and diols, Angew. Chem. Int. Ed. 58 (2019) 557–560.
[52] X. Su, X.-F. Yang, Y. Huang, B. Liu, T. Zhang, Single-atom catalysis toward efficient CO2 conversion to CO and formate products, Acc. Chem. Res. 52 (2019) 656–664.
[53] H. Zhong, M. Iguchi, M. Chatterjee, T. Ishizaka, M. Kitta, Q. Xu, H. Kawanami, Interconversion between CO2 and HCOOH under basic conditions catalyzed by PdAu nanoparticles supported by amine-functionalized reduced graphene oxide as a dual catalyst, ACS Catal. (2018) 5355–5362.
[54] K. Jiang, K. Xu, S. Zou, W.-B. Cai, B-doped Pd catalyst: boosting room-temperature hydrogen production from formic acid–formate solutions, J. Am. Chem. Soc. 136 (2014) 4861–4864.
[55] C. Tisseraud, C. Comminges, A. Habrioux, S. Pronier, Y. Pouilloux, A. Le Valant, Cu-ZnO catalysts for CO2 hydrogenation to methanol: morphology change induced by ZnO lixiviation and its impact on the active phase formation, Mol. Catal. 446 (2018) 98–105.
[56] S. Tada, S. Kayamori, T. Honma, H. Kamei, A. Nariyuki, K. Kon, T. Toyao, K.-i. Shimizu, S. Satokawa, Design of interfacial sites between Cu and amorphous ZrO2 dedicated to CO2-to-Methanol hydrogenation, ACS Catal. 8 (2018) 7809–7819.
[57] S. Tada, A. Katagiri, K. Kiyota, T. Honma, H. Kamei, A. Nariyuki, S. Uchida, S. Satokawa, Cu species incorporated into amorphous ZrO2 with high activity and selectivity in CO2-to-methanol hydrogenation, J. Phys. Chem. C 122 (2018) 5430–5442.
[58] F.M. Auxilia, S. Ishihara, S. Mandal, T. Tanabe, G. Saravanan, G.V. Ramesh, N. Umezawa, T. Hara, Y. Xu, S. Hishita, Y. Yamauchi, A. Dakshanamoorthy, J.P. Hill, K. Ariga, H. Abe, Low-Temperature remediation of NO catalyzed by interleaved CuO nanoplates, Adv. Mater. 26 (2014) 4481–4485.
[59] M.D. Rhodes, A.T. Bell, The effects of zirconia morphology on methanol synthesis from CO and H2 over Cu/ZrO2 catalysts: part I. Steady-state studies, J. Catal. 233 (2005) 198–209.
[60] M.D. Rhodes, K.A. Pokrovski, A.T. Bell, The effects of zirconia morphology on methanol synthesis from CO and H2 over Cu/ZrO2 catalysts: part II. Transient-response infrared studies, J. Catal. 233 (2005) 210–220.
[61] T. Witoon, J. Chalorngtham, P. Dumrongbunditkul, M. Chareonpanich, J. Limtrakul, CO2 hydrogenation to methanol over Cu/ZrO2 catalysts: effects of zirconia phases, Chem. Eng. J. 293 (2016) 327–336.
[62] K. Pokrovski, K.T. Jung, A.T. Bell, Investigation of CO and CO2 adsorption on tetragonal and monoclinic zirconia, Langmuir 17 (2001) 4297–4303.
[63] P.C. Zonetti, J. Celnik, S. Letichevsky, A.B. Gaspar, L.G. Appel, Chemicals from ethanol – the dehydrogenative route of the ethyl acetate one-pot synthesis, J. Mol. Catal. A Chem. 334 (2011) 29–34.
[64] T. Komanoya, K. Nakajima, M. Kitano, M. Hara, Synergistic catalysis by Lewis acid and base sites on ZrO2 for meerwein–Ponndorf–Verley reduction, J. Phys. Chem. C 119 (2015) 26540–26546.
[65] P.M. de Souza, R.C. Rabelo-Neto, L.E.P. Borges, G. Jacobs, B.H. Davis, U.M. Graham, D.E. Resasco, F.B. Noronha, Effect of zirconia morphology on hydrodeoxygenation of phenol over Pd/ZrO2, ACS Catal. 5 (2015) 7385–7398.
[66] H. Jeong, J. Bae, J.W. Han, H. Lee, Promoting effects of hydrothermal treatment on the activity and durability of Pd/CeO2 catalysts for CO oxidation, ACS Catal. 7 (2017) 7097–7105.
[67] C.D. Zeinalipour-Yazdi, D.J. Willock, L. Thomas, K. Wilson, A.F. Lee, CO adsorption over Pd nanoparticles: a general framework for IR simulations on nanoparticles, Surf. Sci. 646 (2016) 210–220.
[68] L. Meng, A.-P. Jia, J.-Q. Lu, L.-F. Luo, W.-X. Huang, M.-F. Luo, Synergetic effects of PdO species on CO oxidation over PdO–CeO2 catalysts, J. Phys. Chem. C 115 (2011) 19789–19796.
[69] B. Bachiller-Baeza, I. Rodriguez-Ramos, A. Guerrero-Ruiz, Interaction of carbon dioxide with the surface of zirconia polymorphs, Langmuir 14 (1998) 3556–3564.
[70] L.-Y. Jin, R.-H. Ma, J.-J. Lin, L. Meng, Y.-J. Wang, M.-F. Luo, Bifunctional Pd/Cr2O3–ZrO2 catalyst for the oxidation of volatile organic compounds, Ind. Eng. Chem. Res. 50 (2011) 10878–10882.
[71] X. Wang, H. Shi, J.H. Kwak, J. Szanyi, Mechanism of CO2 hydrogenation on Pd/Al2O3 catalysts: kinetics and transient DRIFTS-MS studies, ACS Catal. 5 (2015) 6337–6349.
[72] E.-M. Köck, M. Kogler, T. Bielz, B. Klötzer, S. Penner, In situ FT-IR spectroscopic study of CO2 and CO adsorption on Y2O3, ZrO2, and yttria-stabilized ZrO2, J. Phys. Chem. C 117 (2013) 17666–17673.
[73] T. Das, G. Deo, Synthesis, characterization and in situ DRIFTS during the CO2 hydrogenation reaction over supported cobalt catalysts, J. Mol. Catal. A Chem. 350 (2011) 75–82.
[74] H. Takano, Y. Kirihata, K. Izumiya, N. Kumagai, H. Habazaki, K. Hashimoto, Highly active Ni/Y-doped ZrO2 catalysts for CO2 methanation, Appl. Surf. Sci. 388 (2016) 653–663.
[75] C. Schild, A. Wokaun, R.A. Koeppel, A. Baiker, Carbon dioxide hydrogenation over nickel/zirconia catalysts from amorphous precursors: on the mechanism of methane formation, J. Phys. Chem. 95 (1991) 6341–6346.
[76] J. Weigel, R.A. Koeppel, A. Baiker, A. Wokaun, Surface species in CO and CO2 hydrogenation over Copper/Zirconia: on the methanol synthesis mechanism, Langmuir 12 (1996) 5319–5329.